Hindawi
Mathematical Problems in Engineering
Volume 2023, Article ID 7317870, 12 pages
https://doi.org/10.1155/2023/7317870

Research Article

Developing Control Strategy for PV-Based Distributed Generator for Enhancing Frequency Regulation of Microgrid

Hoang Minh Vu Nguyen [1] **and Trong Nghia Le** [2]

[1]*HCMC University of Architecture, Ho Chi Minh City 72407, Vietnam*
[2]*Electrical and Electronics Engineering Department, HCMC University of Technology and Education, Ho Chi Minh City 71313, Vietnam*

Correspondence should be addressed to Hoang Minh Vu Nguyen; vu.nguyenhoangminh@uah.edu.vn

Received 4 August 2023; Revised 15 September 2023; Accepted 30 October 2023; Published 27 November 2023

Academic Editor: Wesley Peres

This paper presents a control strategy for a photovoltaic (PV)-based distributed generator (DG) to enhance the frequency regulation of a microgrid. A microgrid is a small-scale power system that integrates distributed energy sources and interconnected loads, which can operate independently or in parallel with the main grid. However, the high integration of DGs poses stability problems, particularly the frequency regulation under contingencies in the microgrid. For example, the shutdown of one generating unit or the reduction of system inertia owing to the high integration of converter-based DGs will increase the risk of instability of the microgrid and the main grid. Therefore, maintaining and increasing the frequency regulation capability is crucial in microgrid operation. This paper focuses on developing a controller for PV DG based on virtual inertia control combined with the conventional control method of a converter in order to regulate the microgrid frequency under contingency. The proposed control strategy for a PV-based DG is then verified through simulation of the 14-bus microgrid model using MATLAB/Simulink, showing regulation in frequency under island mode operation of the microgrid. In addition, comparisons between the original and proposed control strategy microgrid model are then carried out.

1. Introduction

Microgrid is a small-scaled, independent, controllable electrical system consisting of distributed generators (DGs), load, energy storage systems (ESSs), and other ancillary devices. Microgrid can operate in grid-connected mode or in islanding mode. Compared with the traditional power system, microgrid will be more optimal and flexible [1–4]. DGs in microgrid include two main groups; the first one is converter-based DGs, including photovoltaic (PV) [5–11], Wind [10–15], and hydrogen batteries [11]; the second group is conventional DG based on traditional synchronous generators, such as gas turbines, small steam turbines, and diesel generators [11]. Loads in the microgrid include shared loads and separate loads. And ESSs include fuel cells, battery energy storage (BES), Flywheel energy storage systems [16].

Traditionally, the various DGs in microgrid (MG) are usually applied using a singular conventional control method, e.g., maximum power point tracking (MPPT) through an inverter [17–19]. This control strategy is currently given limitations compared to the system that applies various control methods, such as frequency variation with high amplitude and long steady-state period under unintentional grid disconnection and/or connecting heavy loads, or may breakdown the whole microgrid under critical faults, etc. Some of the methods that have been conducted in frequency regulation in microgrid can be listed as follows: *P*/*Q* control method [17, 18] helps regulated the system frequency through adjusting the DG's active output power; however, its limitation is the supporting control feature; *U*/*f* control [16, 20] helps to regulate the voltage and frequency at the point of common coupling (PCC) through droop controllers of the active and reactive power of the DGs, the inability to control DG's responses in accordance to the rate of change of voltage and frequency under contingency is the main limitation of this control method [20, 21]; another well-known control method

that is widely applied is virtual inertial control [22–25], which changes the power output of converter-based DG according to the rate of change of frequency at (PCC). However, the limitation in finding the virtual coefficient of inertia [22, 26] and the required energy reserve of converter-based DG to implement this control strategy [26] are currently a barrier in its system-scale application, which is also the target for studying. This paper presents developing a controller for PV DG based on virtual inertia control combined with the conventional control method of a converter in order to enhance the frequency regulation of the microgrid under contingency.

This paper includes five sections; Section 2 presents the principles of microgrid frequency control and then proceeds to develop a control strategy for PV-based DG to support frequency regulation in microgrid, as shown in Section 3. The verification of the proposed converter control strategy through simulation results and comparison to the original model using MATLAB/Simulink model is presented in Section 4. Finally, the conclusion is given in Section 5.

2. Control Methods of Converter-Based DG for Frequency Regulation in Microgrid

Microgrids can function in either a grid-connected or standalone mode. In grid-connected mode, the DGs within the microgrid operate with a standard maximum power generation approach, typically using P/Q control methods. This ensures power balance and efficient utilization of renewable energy resources. The microgrid's rated voltage and frequency are supported and regulated by the main power grid since the microgrid's total capacity is significantly smaller. In standalone mode, to maintain the microgrid's rated voltage and frequency, one or more DGs must act as grid-forming sources. These grid-forming DGs utilize U/f control and droop control methods to supply the required voltage and frequency to other DGs within the microgrid [5, 16, 27].

2.1. dq0 Synchronous Reference System with Converter Control. In the controller design phase or in the operating analysis of the power converter, the equations describing the voltage and current of the converter connected to an AC bus via a filter must be derived. For example, basic equations describing the mentioned system are as follows [28]:

$$V_{\text{abc}} = R.i_{\text{abc}} + L\frac{d}{dt}i_{\text{abc}} + V_{\text{abc,conv}}, \tag{1}$$

where V_{abc}: AC voltages represented in a three-phase format (a, b, c); i_{abc}: AC currents represented in a three-phase format (a, b, c); $V_{\text{abc,conv}}$: AC voltage at the input of the converter; R: resistance between the converter and the AC system; L: filter inductance between the converter and the AC system.

In order to determine the coefficients in the control designed phase, the converter's three-phase current and voltage, it needs to be transformed into a two-axis dq reference frame, which synchronously rotates at the microgrid frequency (ω). The voltage equations in the dq synchronous reference frame, obtained using the Clark–Park transform, can be written as follows [28]:

$$\begin{aligned} L\frac{d}{dt}i_d &= -Ri_d + \omega Li_q - V_{d,\text{conv}} + V_d \\ L\frac{d}{dt}i_q &= -Ri_q - \omega Li_d - V_{q,\text{conv}} + V_q. \end{aligned} \tag{2}$$

The angular position of the voltage vector is determined by the equation as follows:

$$\theta = \tan\left(\frac{v_\alpha}{v_\beta}\right), \tag{3}$$

where v_α and v_β represent the components of voltage in the stationary two-axis reference frame (Clark's transform). The angle θ can be computed using a phase lock loop (PLL) technique.

2.2. P/Q Control Method. The primary function of the converter is to regulate and control the output of active and reactive power. In the P/Q control method, the converters are designed to generate active and reactive power according to predetermined set values or reference values. This control strategy allows for precise management and adjustment of the active and reactive power output to meet specific system requirements and maintain the desired power balance within the microgrid or power system [16]. Furthermore, the P/Q control is also derived for partly frequency support of the power converter using system equation analysis. As mentioned in the previous section, the three-phase voltage of converter-interfaced DG in a synchronous reference frame is derived as follows:

$$v_d = Ri_d + L\frac{di_d}{dt} - \omega Li_q + u_d, \tag{4}$$

$$v_q = Ri_q + L\frac{di_q}{dt} + \omega Li_d + u_q, \tag{5}$$

where u_d and u_q are the voltage at the converter terminal; ωLi_q and ωLi_d are cross-coupling components.

PI controllers are widely used for outer loop power control. By deriving the PI controller, the reference signals for the outer loop power control can be given as follows:

$$i_{\text{dref}} = (P_{\text{ref}} - P)\left(k_{p1} + \frac{k_{i1}}{s}\right), \tag{6}$$

$$i_{\text{qref}} = (Q_{\text{ref}} - Q)\left(k_{p3} + \frac{k_{i3}}{s}\right), \tag{7}$$

where P_{ref} and Q_{ref} are the reference active and reactive power, respectively; i_{dref} and i_{qref} are the d-axis and q-axis reference currents, respectively.

When the grid voltage remains constant, the converter's outputs are influenced by the reference current. The active

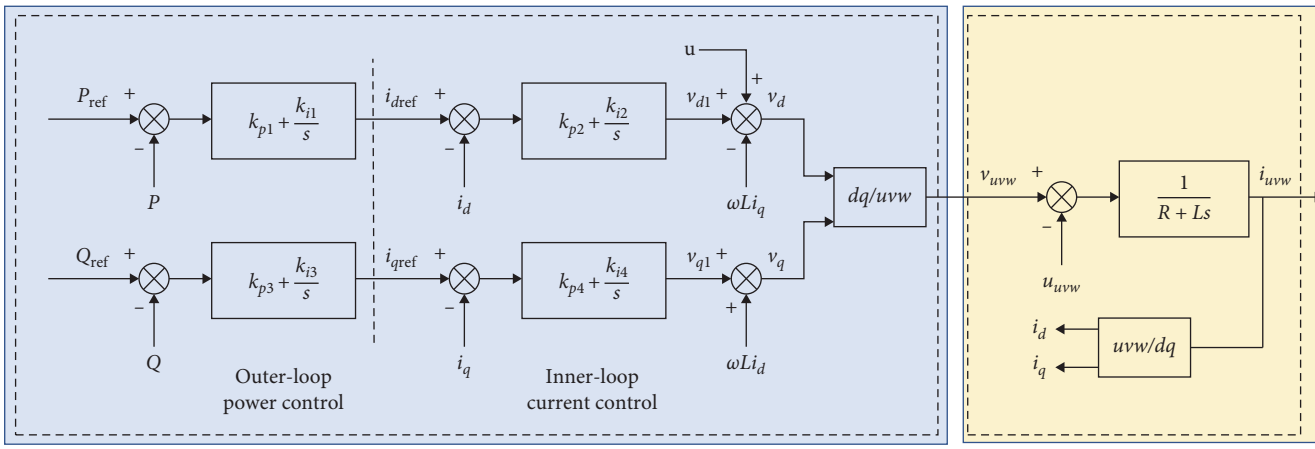

FIGURE 1: P/Q control diagram.

power output is proportional to the d-axis current (i_d), while the reactive power output is proportional to the q-axis current (i_q). By controlling and adjusting the reference currents, the converter can regulate the active and reactive power, which then helps to maintain the desired power flow and stable dynamic performance.

The transfer function between v_{d1}/v_{q1} and i_d/i_q is first-order hysteresis. It is possible to design an internal loop current controller, usually by a PI controller. As shown in Figure 1 [16], the mathematical model of the current PI controller is shown as follows [28]:

$$v_{d1} = (i_{\text{dref}} - i_d)\left(k_{p2} + \frac{k_{i2}}{s}\right), \tag{8}$$

$$v_{q1} = (i_{\text{qref}} - i_q)\left(k_{p4} + \frac{k_{i4}}{s}\right). \tag{9}$$

By adding offsets, it becomes possible to eliminate the impact of mains voltage and cross-coupling d_q, enabling current separation control. The reference voltage for pulse width modulation (PWM) is derived by applying the inverse Clark–Park transform. Subsequently, PWM is employed to generate the three-phase output voltage of the converter. Figure 1 illustrates this process [16].

2.3. U/f Control Method. In the *U/f* control method, the inverter is responsible for generating a constant voltage and frequency to ensure the uninterrupted operation of auxiliary DGs and sensitive loads when the microgrid is disconnected from the main power system or operating in standalone mode. In standalone operation, the microgrid has limited power generation capacity. Therefore, in the event of a power shortage, it becomes necessary to shed nonessential loads to ensure continuous power supply to critical loads [29].

In the *U/f* control mode, the AC voltage on the microgrid side is adjusted based on feedback signals to maintain a constant output. This is typically achieved through a dual-loop control scheme, consisting of an outer loop voltage control and an inner loop current control. The outer loop voltage control helps to stabilize the output voltage, while the inner loop current control works in conjunction with it to expedite the recovery process and safeguard the microgrid against disturbances [30]. In addition, the cross-coupling terms considering filter parameters (inductance L_f and capacitance C_f) are derived in the voltage and current control phases. This combined control approach ensures the stability and protection of the microgrid system during operation. Figure 2 illustrates this process.

2.4. Droop Control Method. Droop control is implemented by emulating the behavior of traditional generators in a conventional grid. This involves adjusting the output voltage and frequency of the converter based on changes in the output power. In a microgrid, where multiple DGs are connected through converters, operating off-grid is equivalent to having multiple converters connected in parallel. As a result, the active and reactive power of each converter can be determined using the following principles [5]:

$$Pn = \frac{UU_n}{X_n}\sin\delta_n, \tag{10}$$

$$Qn = \frac{UU_n\cos\delta_n - U^2}{X_n}, \tag{11}$$

where U: bus voltage; U_n: output voltage of the inverter power supply; X_n: output impedance, typically referring to the filter impedance; δ_n: deviation angle between U_n and U.

Based on Equations (10) and (11), the power distribution in the droop control scheme is influenced by δ_n, while the reactive power is primarily determined by the output voltage amplitude of the inverter, U_n. The phase difference between the output voltage and the bus voltage can be regulated by adjusting the angular frequency of the inverter, which can be done using the following equation:

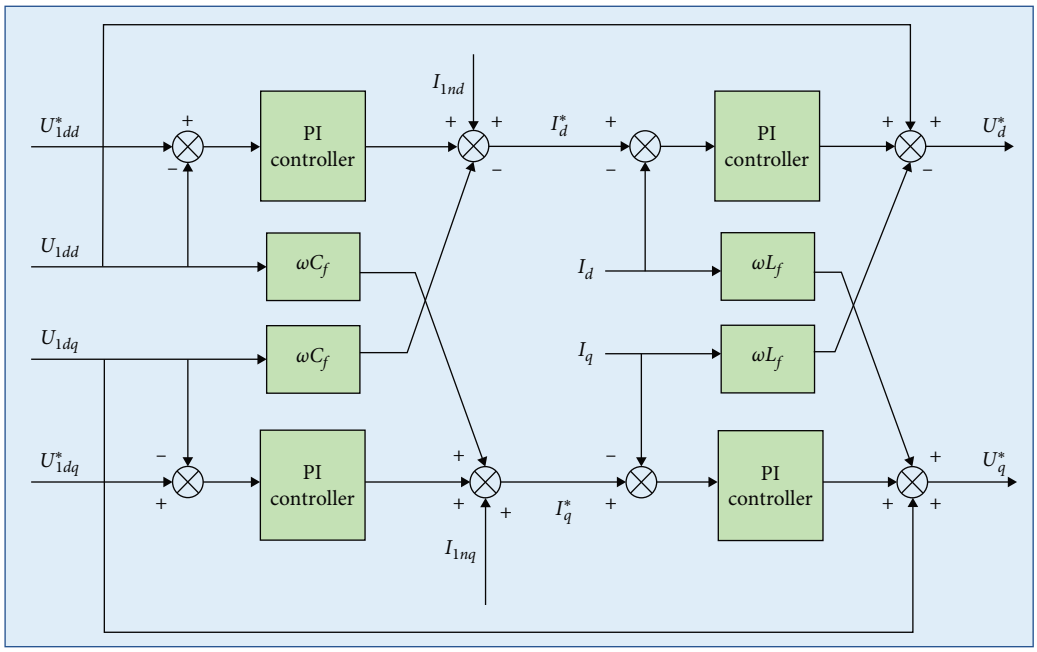

Figure 2: *U*/*f* control diagram.

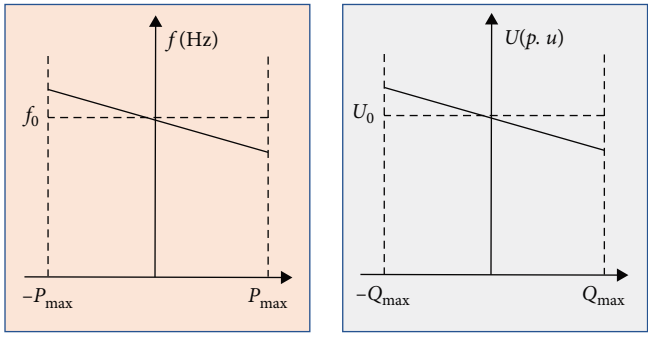

Figure 3: *P*–*f* and *Q*–*u* characteristic curves in droop control method [6].

$$f_n = \frac{\omega_n}{2\pi} = \frac{d\delta_n}{2\pi dt}. \tag{12}$$

As in Equations (10)–(12), the voltage and power of the converter can be adjusted by measuring the voltage amplitude and frequency of the connected bus according to a predefined curve from which the active and reactive power of the converter are adjusted through the droop gain and deviation from the rated voltage and frequency, as shown in Figure 3.

2.5. Virtual Inertia Control. The inertia of a synchronous generator is that when a change in frequency occurs, the machine will react by accelerating or decelerating in order to transfer the kinetic energy stored in the rotating mass of the machine to the support the grid. As the frequency increases, the rotational speed of the machine also increases to absorb kinetic energy and vice versa. Then, the governor of the synchronous machine will increase or decrease the mechanical power to adjust the output power and then adjust the frequency. However, in the highly integrated converter-interfaced DG microgrid with the overall system inertia being low [22–25], the virtual inertia control strategies have been studied and derived as an alternative control method to improve the low inertia properties of microgrid. However, the application of virtual inertia control combined with droop control for converter interfaced DGs considering the factors such as voltage, frequency, and the unintentional islanding phenomenon of the microgrid has not been mentioned in other studies, which leads to the main research objective of this paper. Figure 4 shows the general control scheme of virtual inertia of a converter-based DG.

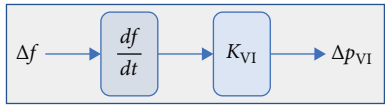

Figure 4: General control diagram of virtual inertia in a converter-based DG.

Equation (13) shows the relationship between the input and output control quantities of a DG when applying the virtual inertial control strategy:

$$\Delta p_{v1} = K_{v1}\frac{df}{dt} = K_{v1}\frac{\Delta f}{\Delta t}. \tag{13}$$

3. Developing the Control Strategy for PV-Based DG to Support Frequency Regulation in Microgrid

In order to verify the control strategy for PV-based DG supporting frequency regulation in microgrid proposed in

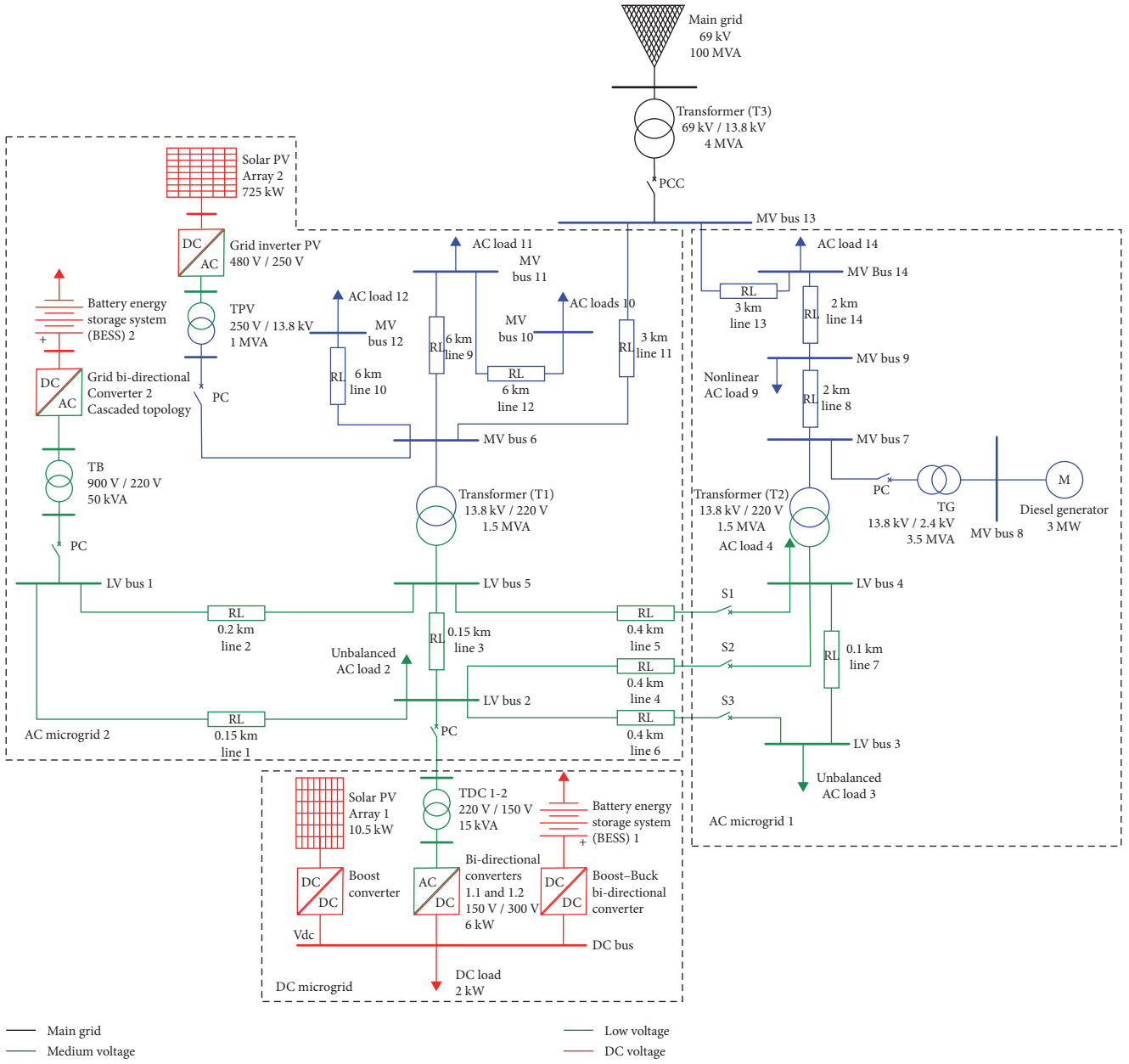

FIGURE 5: General control diagram of virtual inertia in a converter-based DG [32].

this paper, a 14-bus microgrid model will be derived for simulation using MATLAB/Simulink. The model provides some basic research cases, such as reactive power compensation, inertial analysis and stability, reliability, hierarchical control, optimization strategy, and energy storage, especially for the studying of frequency response [31].

In Figure 5, the microgrid used in the simulation has two distribution voltage levels: the primary voltage level of 13.8 kV is depicted in the blue line, and the secondary voltage level of 0.22 kV is shown in the green line. The three subgrids include AC MG 1, which is the area connected at 0.22 kV via distribution lines 4, 5, and 6 to AC MG 2. Distributed sources in the microgrid include 1 BESS DG, 1 PV DG, and 1 Diesel DG that connect to the AC busbar, 1 PV DG and 1 BESS connect to the DC busbar, and a central converter acts as the main interface between the microgrid and the AC power system.

In the converter control unit, an MPPT controller for maximum power detection, voltage and current controllers, PLLs, and PWM signal generators to generate the preference control voltage. All of which are widely used in converter control, details shown in Figure 6.

In this section, a new control strategy with the capability of adjusting the output active power according to the rate of change and deviation of system frequency and adjusting the reactive power according to the setting values and/or to the terminal voltage magnitude will then be applied in the PV-based grid inverter control system to which connected to "MV Bus6" in Figure 5.

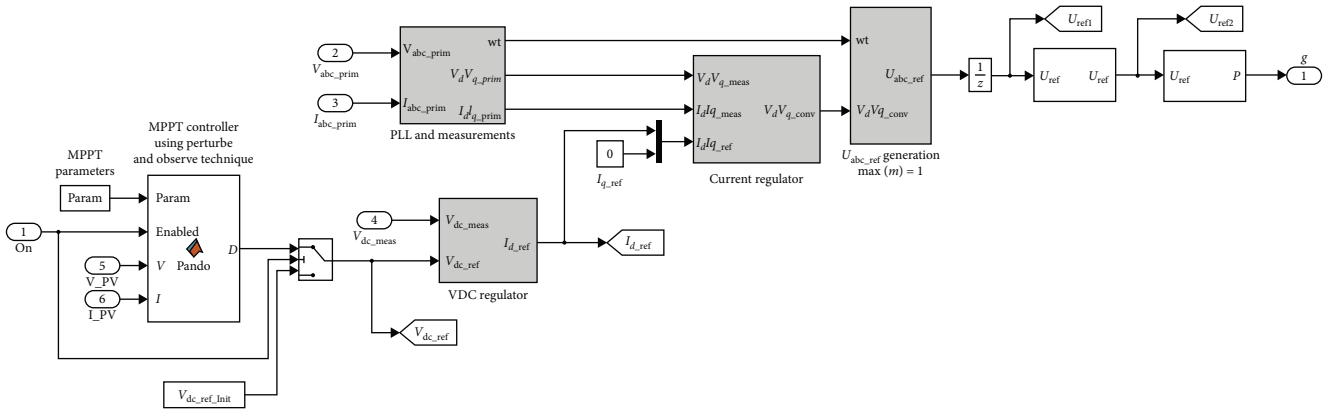

Figure 6: Connection diagram inside the converter control block.

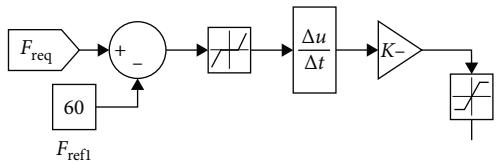

Figure 7: The inertia control stage of the new controller.

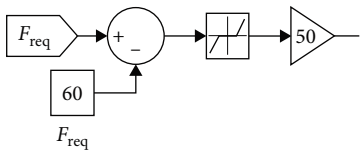

Figure 8: The inertia control stage of the new controller.

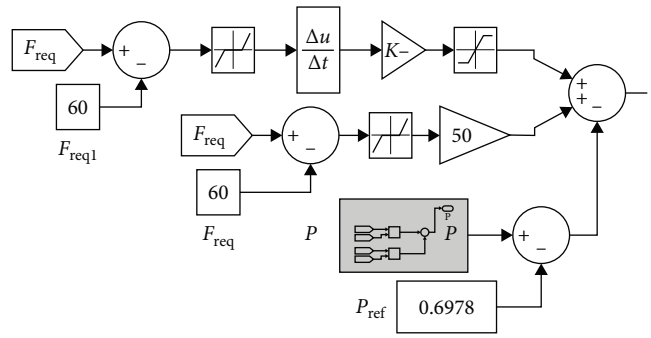

Figure 9: Connection diagram of signal generator block V_{od_ref}.

Figure 7 shows the block diagram of the virtual inertial control strategy applied to PV-based DG with the capability of regulating the output active power following the rate of change of frequency.

Another requirement of the controller is the ability to adjust the active power under frequency deviation, as shown in Figure 8. The frequency errors can pass through the dead zone block to avoid interference with the control signal and then through the Gain block for amplification, which acts as the droop control function mentioned in Section 2.4.

The proposed controller also requires the ability to adjust the active power to the setting value; the instantaneous output powers of the converter are calculated as in Equations (14) and (15) [26]:

$$p = v_d i_d + v_q i_q, \tag{14}$$

$$q = v_d i_q - v_q i_d, \tag{15}$$

where v_d and v_q are the output voltage in the dq reference frame; i_d and i_q are the axis shifting current in the dq reference frame [29].

Figure 9 shows the block diagram of signal generator blocks. Then, using a traditional PI controller for the voltage and current control loop combined with compensating components of grid voltage and cross-coupling, then the reference voltage values V_{d_ref} and V_{q_ref} are obtained. Applying the inverse Clark–Park transform and a PWM generator to generate switching signals of the converter, the details are shown in Figures 10 and 11. The coefficients k_p and k_i of the current and voltage controllers are determined by trial-and-error method.

Figure 12 shows a general model of a PV-based DG with the controller modified according to the proposed method.

4. Simulation Results

The simulations are conducted on a 14-bus microgrid model between the PV-based DG with the original controller (Model 1) and PV-based DG with the proposed control strategy (Model 2). The whole simulation time lasts for 1 s. The microgrid is initially in grid-connected mode; from 0.32 s, the MG is disconnected from the main grid and operated in island mode. The frequency variation of microgrid is then compared between two models. Parameters of the original model are given in Tables 1–3 with details by Ortiz et al. [32], and the controller parameters of the proposed control strategy of Model 2 are shown in Table 4.

4.1. Frequency Waveform at AC PV Bus. At 0.32 s after disconnecting from the power grid, a slide decreasing followed by high increasing in frequency variations occurred at two models, for specific, Model 1, which has the PV-based DG controlled in MPP mode, the frequency increases with a

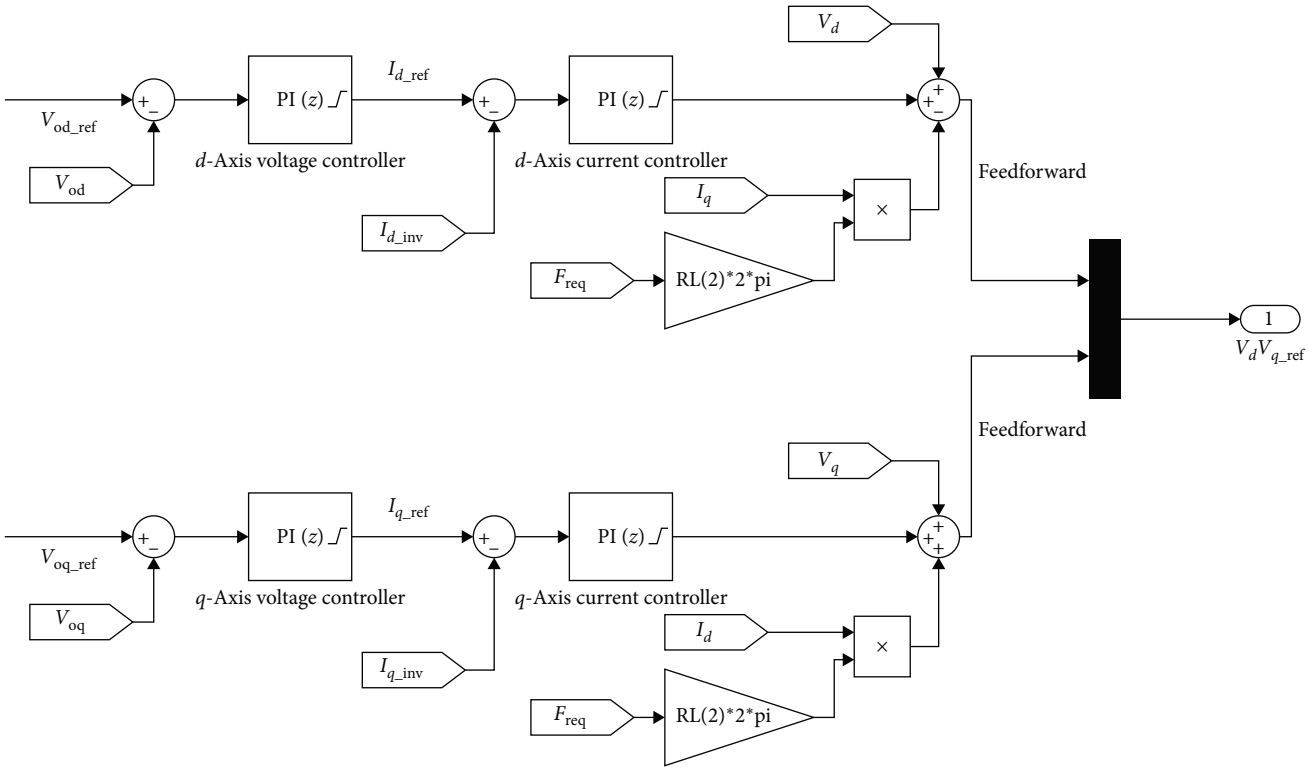

Figure 10: Diagram of reference control signal generation.

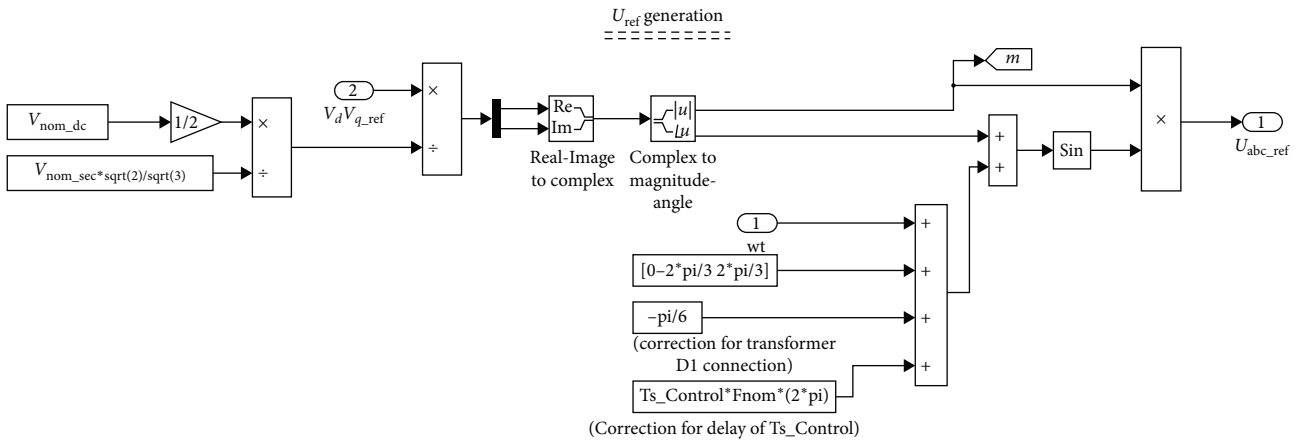

Figure 11: Diagram of reference voltage applied in PWM generation.

higher value (60.08 Hz) than that of the Model 2 (60.06 Hz) where the proposed control strategy is applied. Furthermore, after 0.36 s, the frequency tends to become unstable, with variations occurred at a steady state in Model 1, as shown in Figure 13(a). In contrast, Figure 13(b) shows frequency variation in Model 2 with a lower value when frequency increases and gets to a steady state fast with seamless variations to the rated value of 60 Hz.

4.2. Power Waveforms (P, Q) at the AC PV Bus. At 0.32 s after disconnecting from the power grid, in Model 2, the active output power P has the adjustment of generating from 0.32 to 0.37 s under frequency decreasing, which supports balancing power in the microgrid, as shown in Figure 14(b). However, in Model 1, the active output power P is always transmitted at the maximum value since the MPPT control method was applied, as shown in Figure 14(a). Furthermore, the proposed controller is able to adjust the reactive power Q generation, which then supports voltages of the microgrid more stable under Island mode operation, as shown in Figure 14(b).

4.3. Power Waveforms (P, Q) at Main Grid. Before disconnecting to the utility, as in Figure 15, the main grid transmitted more active power to the microgrid in Model 2 (Figure 15(a)) than that of Model 1 (Figure 15(b)). Since in

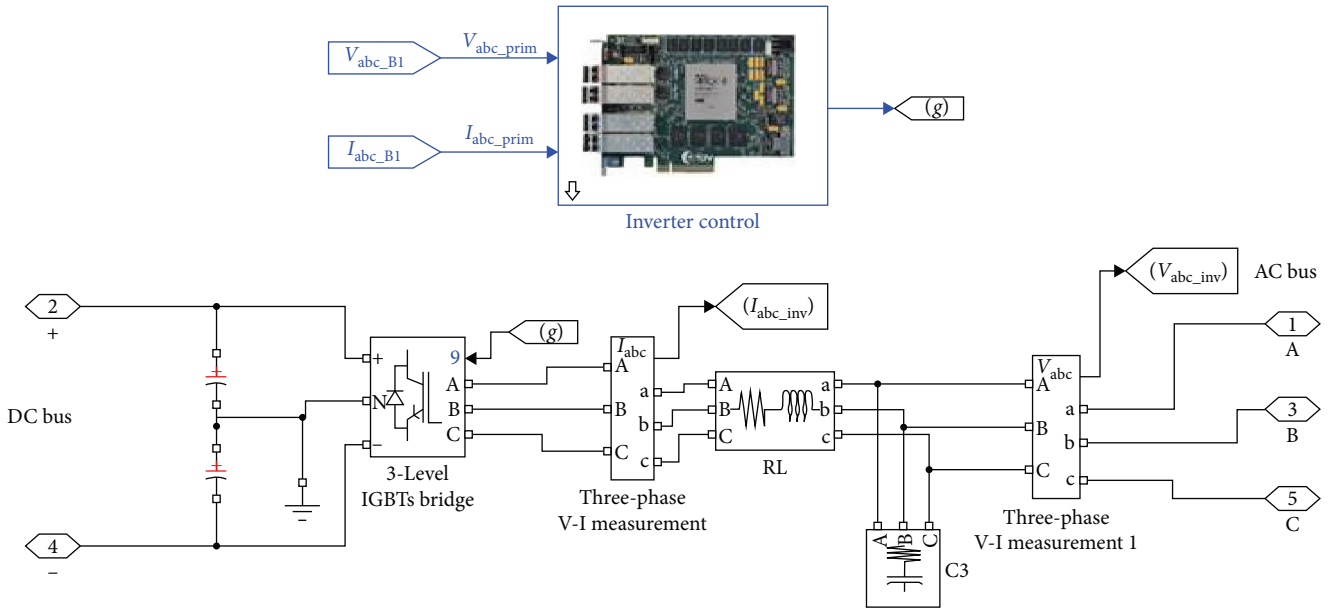

Figure 12: MATLAB/Simulink model of the PV-based DG using the proposed control strategy.

Table 1: Transformer ratings.

Transformer	Power (kVA)	Voltage Ratio (HV/LV)	R_{cc} (pu)	X_{cc} (pu)
T1	1500	Y13800/220Y	3	3
T2	1500	Y13800/220Y	3	3
T3	4,000	YG69000/13800D1	15	15
TB	55	D1900/220Y	3	6
TG	3,500	Yg13800/2400D1	15	15
TPV	1,000	Yg13800/250D1	12	3
TDC1–2	15	Y220/150Y	3	6

Table 2: Line data.

Line	Sending end	Receiving end	R (ohm)	X (ohm)	Distance (km)
1	LV1	LV2	0.0297	0.016335	0.15
2	LV1	LV5	0.0396	0.02178	0.2
3	LV2	LV5	0.0297	0.016335	0.15
4	LV2	LV4	0.0792	0.04356	0.4
5	LV4	LV5	0.0792	0.04356	0.4
6	LV2	LV3	0.0792	0.04356	0.4
7	LV3	LV4	0.0198	0.01089	0.1
8	MV7	MV9	0.788	0.2336	2.0
9	MV6	MV11	2,364	0.7008	6.0
10	MV6	MV12	2,364	0.7008	6.0
11	MV6	MV13	1.182	0.3504	3.0
12	MV10	MV11	2,364	0.7008	6.0
13	MV13	MV14	1.182	0.3504	3.0
14	MV9	MV14	0.788	0.2336	2.0

Table 3: Load data in the microgrid.

Bus ID	Load name	Load type	Max load (kVA)	Min load (kVA)	PF	Unbalance load (%)
LV2	Load 2	Unbalanced load	40	12	0.9	13
LV3	Load 3	Unbalanced load	30	9	0.85	12.6
LV4	Load 4	Linear load	50	15	0.9	0
MV9	Load 9	Non-linear load	320	96	0.1	0
MV10	Load 10	Linear load	800	240	0.8	0
MV11	Load 11	Linear load	400	120	0.8	0
MV12	Load 12	Linear load	800	240	0.8	0
MV14	Load 14	Linear load	1,600	480	0.8	0
DC	DC	—	2 (kW)	6 (kW)	1	—

Table 4: Converter parameters of the proposed control strategy.

Parameters	Description	Value
K_{pv}	Voltage controller's proportional gain	2
K_{iv}	Voltage controller's integral gain	3,000
K_{pc}	Current controller's proportional gain	0.3
K_{ic}	Current controller's integral gain	200
R_f	Inverter filter resistance in pu	0.0015
L_f	Inverter filter inductance in pu	0.15
K	Virtual inertia coefficient	2
D	Frequency drop gain	20

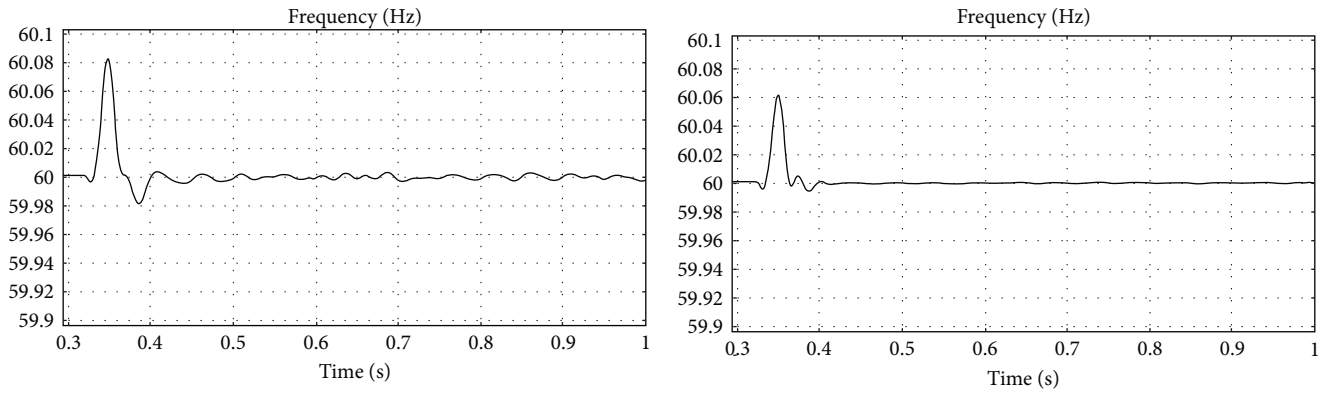

Figure 13: Frequency waveform at AC PV bus the caption: (a) Model 1; (b) Model 2.

Model 2, the PV-based DG with the proposed control strategy is not in the MPPT mode but is reserved for inertia support capability. This capability will then help to regulate the frequency of microgrid more better than that of the original system in Model 1.

4.4. Power Waveforms (P, Q) at BESS Bus. The output powers at the BESS Bus are almost the same. However, there is a slice difference of nearly 200 W lower in the active power output of Model 2 than that of Model 1, as shown in Figures 16(a) and 16(b). The difference in output power between two models comes from the control strategy applied for PV-based converter-interfaced DG, which emulates virtual inertia, resulting in the output power of the PV converter always regulated and adapted to frequency contingency, which then affects the power generation of other DGs.

4.5. Power Waveforms at the AC/DC Buses. As shown in Figure 17(a), the active power transmitted to the DC bus is kept constant about 1 kW in Model 1, and the reactive power generated from the DC bus is more than 200 VAR. At 0.32 s, the active power injected into the DC bus is reduced with an amount of 800 W, and the reactive power is significantly reduced. The same as in Model 2, the active power is reduced, but quite similar to Model 1, at 0.32 s, the active power injected into the DC bus is reduced nearly 300 W. The

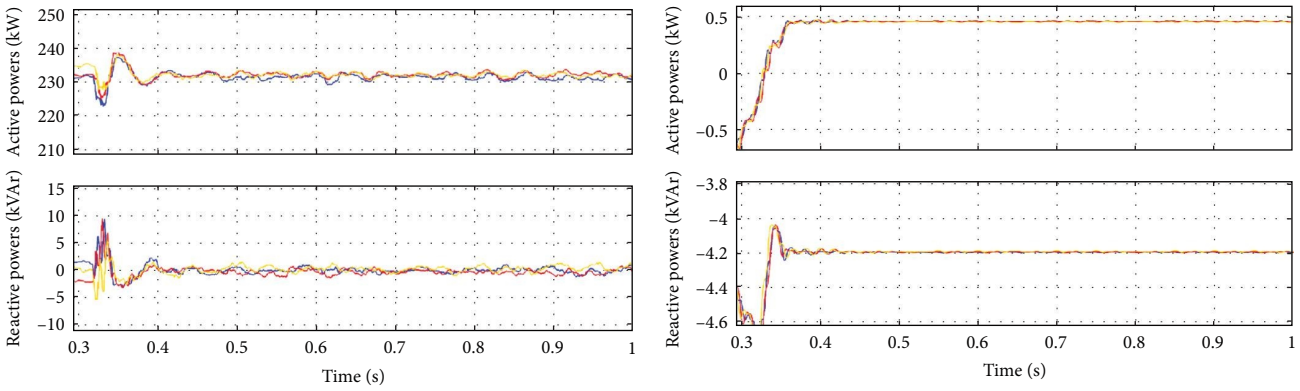

Figure 14: Power waveforms (P, Q) at AC PV bus: (a) Model 1; (b) Model 2.

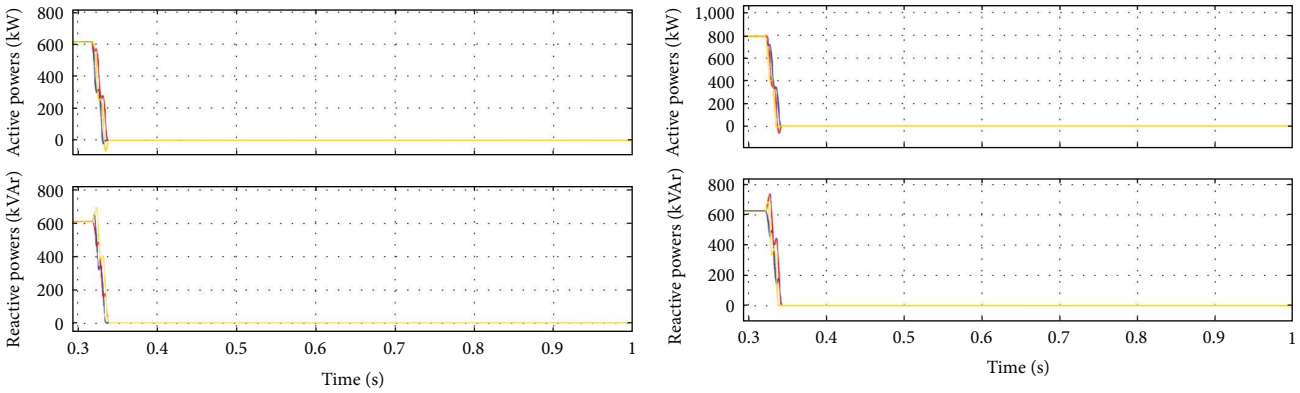

Figure 15: Power waveforms (P, Q) of the main grid: (a) Model 1; (b) Model 2.

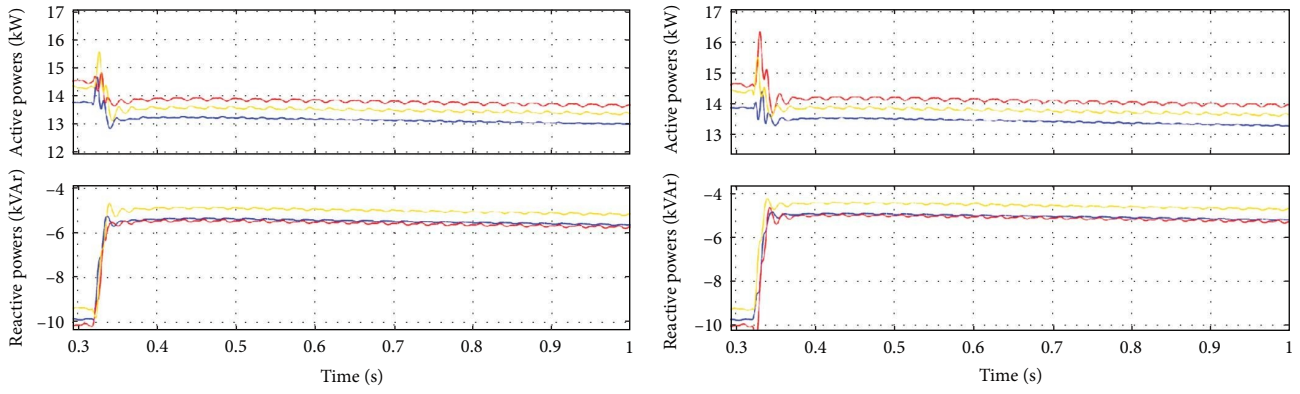

Figure 16: Power waveforms P, Q of BESS: (a) Model 1; (b) Model 2.

difference may come from the control strategy applied for PV-based converter-interfaced DG, which emulates virtual inertia, resulting in the output power of PV converter always regulated and adapted to frequency contingency which then affects the power generation of other DGs. The proposed controller also causes the power balancing (active and reactive) and response little different from the original model (Model 1, Figure 17(a)).

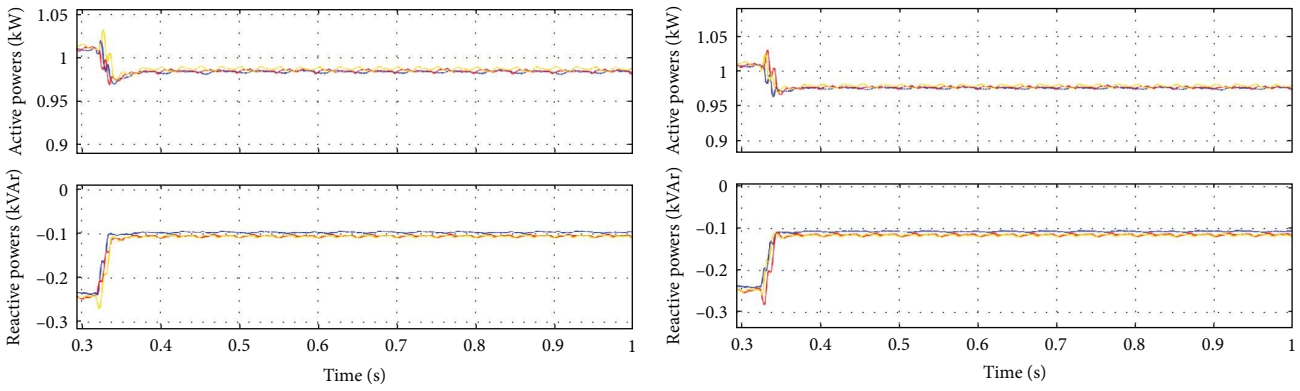

Figure 17: Power waveforms (P, Q) at AC/DC 1: (a) Model 1; (b) Model 2.

5. Conclusions

This paper presents problems related to frequency stability in a highly integrating converter-based DG microgrid and then proposes a control strategy to support frequency regulation under contingency. Through studying the advantages and limitations of different control methods, the paper has devised a control strategy based on droop control combined with virtual inertia control for a converter-interfaced PV DG. The proposed control strategy provides PV-based DG capability in adjusting the output power following the rate of change and deviation of the microgrid's frequency. Through simulation results, the proposed controller provided a good frequency regulation in a steady state after a major power failure. In addition, the change of output power is mainly from the PV-based DG using the proposed control strategy under contingency than other traditional DGs, which archives the desired control target. Furthermore, the microgrid frequency with the proposed control strategy shows better frequency variations under contingency and in steady state, as compared to the original microgrid system.

Data Availability

The data used to support the findings of this study are available from the corresponding author upon request.

Conflicts of Interest

The authors declare that they have no known competing financial interests or personal relationships that could have appeared to influence the work reported in this paper.

Authors' Contributions

All authors contributed to the study conception and design. Topical guidance was performed by Hoang Minh Vu Nguyen. Material preparation, data collection, and analysis were performed by Trong Nghia Le. The first draft of the manuscript was written by Hoang Minh Vu Nguyen, and all authors commented on previous versions of the manuscript. All authors read and approved the final manuscript.

Acknowledgments

This research was supported by the HCMC University of Architecture and the HCMC University of Technology and Education.

References

[1] N. K. Roy and H. R. Pota, "Current status and issues of concern for the integration of distributed generation into electricity networks," *IEEE Systems Journal*, vol. 9, no. 3, pp. 1–12, 2014.

[2] M. G. Dozein, G. Chaspierre, P. Mancarella, P. Panciatici, and T. Van Cutsem, "Frequency response from solar PV: a dynamic equivalence closed-loop system identification approach," *IEEE Systems Journal*, vol. 16, no. 1, pp. 713–722, 2021.

[3] A. O. Prakash and R. N. Banu, "Feature-reduced stability analysis of islanded photovoltaic microgrid inverters," *International Journal of Photoenergy, Hindawi*, vol. 2022, Article ID 7225179, 15 pages, 2022.

[4] U. N. Ekanayake and U. S. Navaratne, "A survey on microgrid control techniques in Islanded mode," *Journal of Electrical and Computer Engineering*, vol. 2020, Article ID 6275460, 8 pages, 2020.

[5] F. Blaabjerg and D. M. Ionel, *Renewable Energy Devices and Systems with Simulations in MATLAB® and ANSYS®*, Taylor & Francis, 2017.

[6] R. Sreega, B. Nandhini, and K. Nithyananthan, "Design and development of automated solar panel cleaner and cooler," *International Journal of Electrical and Electronics Engineers*, vol. 9, no. 2, 2017.

[7] C. Mu, W. Liu, W. Xu, and M. Rabiul Islam, "Observer-based load frequency control for island microgrid with photovoltaic power," *International Journal of Photoenergy*, vol. 2017, Article ID 2851436, 11 pages, 2017.

[8] G. Zhao, T. Cao, Y. Wang, H. Zhou, C. Zhang, and C. Wan, "Optimal sizing of isolated microgrid containing photovoltaic/photothermal/wind/diesel/battery," *International Journal of Photoenergy*, vol. 2021, Article ID 5566597, 19 pages, 2021.

[9] Z. Wu, Y. Hu, J. Wen, F. Zhou, and X. Ye, "A review for solar panel fire accident prevention in large-scale PV applications," *IEEE Access*, vol. 8, pp. 132466–132480, 2020.

[10] Y. Yang, "Advanced Control of Photovoltaic and Wind Turbines Power Systems," in *Advanced and Intelligent Control*

in Power Electronics and Drives, T. Orłowska-Kowalska, F. Blaabjerg, and J. Rodríguez, Eds., vol. 531 of *Studies in Computational Intelligence*, Springer, Cham, 2014.

[11] E. Kabalci, *Hybrid Renewable Energy Systems and Microgrids*, Academic Press, 2020.

[12] G. Lammert, D. Premm, L. D. P. Ospina, J. C. Boemer, M. Braun, and T. Van Cutsem, "Control of photovoltaic systems for enhanced short-term voltage stability and recovery," *IEEE Transactions on Energy Conversion*, vol. 34, no. 1, pp. 243–254, 2019.

[13] Q. A. Alabdali, A. W. M. Bajawi, A. M. Fatani, and A. M. Nahhas, "Review of recent advances of wind energy," *Science and Education Publishing, Sustainable Energy*, vol. 8, no. 1, pp. 12–19, 2020.

[14] M. E. H. Al-Kharbosy, A. A. Ebrahim, and O. N. Soliman, "*Enhancement protection and operation of the doubly fed induction generator during grid fault*," Master Thesis, South Valley University, 2012.

[15] M. Benghanem, A. AlKassem, A. A. Bensaber, and A. Draou, "Supervisory control scheme of a wind farm connected to a hybrid microgrid," *Journal of Electrical and Computer Engineering*, vol. 2022, Article ID 3615307, 15 pages, 2022.

[16] L. Fusheng, L. Ruisheng, and Z. Fengquan, *Microgrid Technology and Engineering Application*, Academic Press, 2014.

[17] T. Esram and P. L. Chapman, "Comparison of photovoltaic array maximum power point tracking techniques," *IEEE Transactions on Energy Conversion*, vol. 22, no. 2, pp. 439–449, 2007.

[18] B. Subudhi and R. Pradhan, "A comparative study on maximum power point tracking techniques for photovoltaic power systems," *IEEE Transactions on Sustainable Energy*, vol. 4, no. 1, pp. 89–98, 2013.

[19] S. Adhikari and F. Li, "Coordinated V-f and P-Q control of solar photovoltaic generators with MPPT and battery storage in microgrids," *IEEE Transactions on Smart Grid*, vol. 5, no. 3, pp. 1270–1281, 2014.

[20] K. S. Rajesh, S. S. Dash, and R. Rajagopal, "Load frequency control of microgrid: a technical review," in *Green Buildings and Sustainable Engineering*, H. Drück, J. Mathur, V. Panthalookaran, and V. Sreekumar, Eds., Springer Transactions in Civil and Environmental Engineering, Springer, Singapore, 2020.

[21] D. Kumar, H. D. Mathur, S. Bhanot, and R. C. Bansal, "Modeling and frequency control of community micro-grids under stochastic solar and wind sources," *Engineering Science and Technology, an International Journal*, vol. 23, no. 5, pp. 1084–1099, 2020.

[22] P. J. D. S. Neto, T. A. D. S. Barros, J. P. C. Silveira, E. R. Filho, J. C. Vasquez, and J. M. Guerrero, "Power management strategy based on virtual inertia for DC microgrids," *IEEE Transactions on Power Electronics*, vol. 35, no. 11, pp. 12472–12485, 2020.

[23] J. Ndirangu, J. Nderu, and G. Irungu, "Impact of variation of virtual inertia and virtual damping on frequency and power angle responses of virtual inertia emulation controlled converter," in *2022 IEEE PES/IAS PowerAfrica*, Kigali, Rwanda, 2022.

[24] J. Pahasa, P. Potejana, and I. Ngamroo, "MPC-based virtual energy storage system using PV and air conditioner to emulate virtual inertia and frequency regulation of the low-inertia microgrid," *IEEE Access*, vol. 10, pp. 133708–133719, 2022.

[25] T. Kerdphol, F. S. Rahman, M. Watanabe, Y. Mitani, and D. P. H. Turschner Beck, "Enhanced virtual inertia control based on derivative technique to emulate simultaneous inertia and damping properties for microgrid frequency regulation," *IEEE Access*, vol. 7, pp. 14422–14433, 2019.

[26] H. Akagi, E. H. Watanabe, and M. Aredes, *The Instantaneous Power Theory*, Instantaneous Power Theory and Applications to Power Conditioning, IEEE, 2017.

[27] N. Hatziargyriou, *Microgrids Architectures and Control*, IEEE Press, 2014.

[28] C. Bajracharya, M. Molinas, J. Suul, and T. Undeland, "Understanding of tuning techniques of converter controllers for VSC-HVDC," in *Nordic Workshop on Power and Industrial Electronics*, 2008.

[29] J. Rocabert, A. Luna, F. Blaabjerg, and P. Rodríguez, "Control of power converters in AC microgrids," *IEEE Transactions on Power Electronics*, vol. 27, no. 11, pp. 4734–4749, 2012.

[30] A. Fathi, Q. Shafiee, and H. Bevrani, "Robust frequency control of microgrids using an extended virtual synchronous generator," *IEEE Transactions on Power Systems*, vol. 33, no. 6, pp. 6289–6297, 2018.

[31] A. Abdlrahem, G. K. Venayagamoorthy, and K. A. Corzine, "Frequency stability and control of a power system with large PV plants using PMU information," in *North American Power Symposium (NAPS)*, pp. 1–6, 2013.

[32] L. Ortiz, R. Rozonda, A. Aguila, J. W. Gonzalez, G. J. Lopez, and I. Isaac, *Hybrid AC/DC Microgrid Test System Simulation: Grid-Connected Mode*, Hylion, Elsevier, 2019.